



Brussels, Date 27<sup>th</sup> May 2013

Authors: Antonio Garcia-Uceda Juárez  
Thomas Deconinck  
Charles Hirsch

## 2<sup>nd</sup> International Workshop on Higher-Order CFD Methods

NUMECA Int., Chaussée de la Hulpe 189 Terhulpe Steenweg,  
BE - 1170 Brussels, Belgium  
Tel.: [+32 \(0\)2 6478311](tel:+3226478311), Fax.: [+32 \(0\)2 6479398](tel:+3226479398)  
[www.numeca.com](http://www.numeca.com)

### 1. Code description.

The solver employed to obtain the results presented corresponds to the novel Higher-order Flux-Reconstruction (FR) method. This methodology solves the governing equations of the flow directly in its differential form, hence it can be considered as Finite Differences solver, but with some features typical of DG Finite Elements methods. Indeed, the solution  $u(x)$  within each cell (or element in the proper FE nomenclature) is assumed as approximated by a polynomial  $u(x)$  of degree  $K$ , which is in general discontinuous at the interfaces (similarly to DG methods). When solving the governing equations in its differential form, continuity must be assured for the flux function  $F(U)$ , in order to compute the spatial derivatives. However, since this function is also discontinuous at the interfaces, some correction must be applied. As in general Higher-order FE methods, the order of accuracy is determined by the order of the interpolating polynomial  $u(x)$ . However, FR methods offer the advantage of lower computational cost per iteration, since no Gauss integration is needed to compute the integrals encountered in FE methods.

The FR method has been implemented in the NUMECA's solver FINE<sup>tm</sup>/OPEN, as part of PhD project thesis. At this early stage, the solver for Euler equations has been implemented and validated, for any value of degree  $K$  desired (in practice, the maximum order tested is  $K=3$ ). The Euler equations are integrated in time by explicit Runge-Kutta scheme (4<sup>th</sup> order), with no acceleration technique available so far. Thus, the FR solver suffers from the constraint of very low CFL number for higher  $K$ , as well as non-monotone rates of convergence, which hinders greatly the performance of the solver. For this reason, no work units data are displayed below in this report.

---

**n.v. NUMERICAL MECHANICS APPLICATIONS INTERNATIONAL s.a.**

Office address : Chaussée de la Hulpe, 189, Terhulpesteenweg - 1170 Brussels - Belgium

[www.numeca.com](http://www.numeca.com) - Tél: +32 2 647 83 11 - Fax: +32 2 647 93 98 - BTW-TVA:BE 0447 480 893

Bank Accounts : BNP Paribas Fortis : 210-0420 099-44 - Dexia : 068-2406 673-33

## 2. Summary of Cases.

### 2.1. C1.1. Internal inviscid flow over a smooth bump.

#### *Meshes.*

The meshes employed have been generated with NUMECA's software HEXPRESS. The computational domain occupies the range  $-1.5 < x < 1.5$ , and  $0 < y < 0.8$ . Five meshes are used, where each refinement level is generated by splitting each cell of the immediate coarser level into four cells of same size. Hence, meshes of 32, 128, 512, 2048, 8192 number of cells result, with cells slightly clustered around the bump in x-direction. The mesh of 2048 cells is shown in Figure 1:

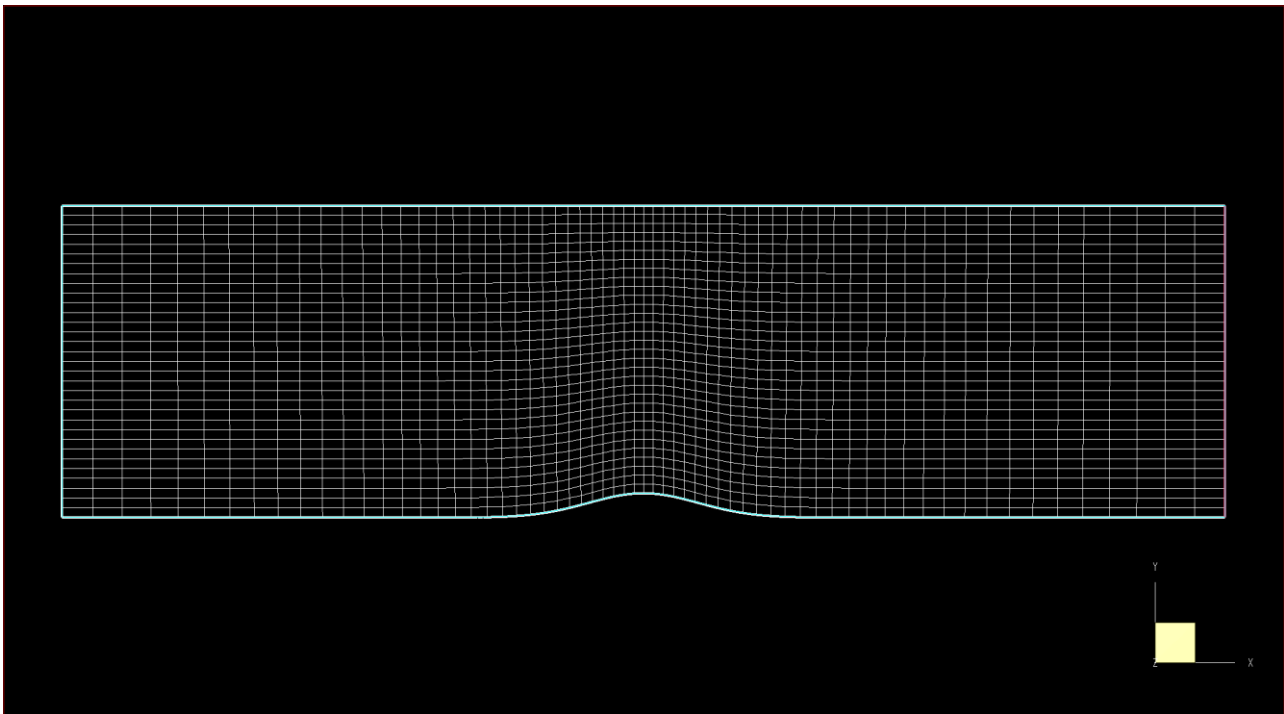


Figure 1: Mesh of 2048 cells generated for test case C1.1.

#### *Problem Set-Up.*

At the left boundary the Mach number of 0.5 is imposed by fixing the total flow properties of Total Pressure  $P_t$  and Temperature  $T_t$ . At the right boundary the pressure is fixed, being the rest of variables extrapolated from inner conditions. Finally, at lower and upper boundaries, mirror boundary conditions are imposed, where normal velocity component to the boundary is set to zero. The solution convergence is assumed when density residuals drop below  $10^{-10}$  (relative to residual at first time step).

## Results.

The level of accuracy is estimated through the L2 norm of the Entropy error. The Figure 2 displays the results obtained as function of number of degrees of freedom ( $h \sim \sqrt{NDof}$ , for 2D case). Moreover, the convergence rates for each K value are summarised in the Table 1. Notice that for K=2, 3, some L2 norm values are not displayed, due to convergence issues encountered.

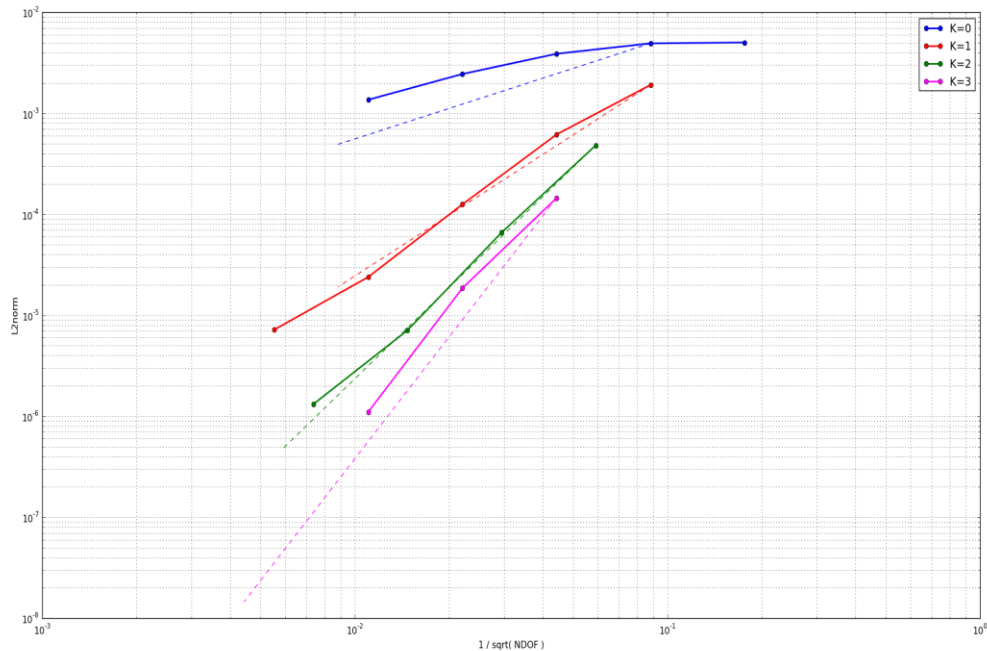


Figure 2: Convergence rates for test case C1.1. obtained with K=0 (blue), K=1 (red), K=2 (green), K=3 (violet). The theoretical slope for each case is sketched as discontinuous line.

<i>Value K</i>	<i>Convergence Rate</i>
0	0.845
1	1.736
2	2.430
3	4.070

Table 1: Convergence rates computed for test case C1.1.

## 2.2. C1.5. Radial expansion wave.

### *Meshes.*

The meshes employed have been generated with NUMECA's software HEXPRESS. These correspond to cartesian meshes, covering the computational domain  $-4 < x, y < 4$ , of constant mesh size throughout it. Four meshes are used, where each refinement level is generated by splitting each cell of the immediate coarser level into four cells of same size. Hence, meshes of 32x32, 64x64, 128x128, 256x256 number of cells result.

## Problem Set-Up.

At all boundaries supersonic boundary conditions are imposed, so that all flow variables are extrapolated from inner conditions. For each simulation run, the time step is set small enough so that errors due to time discretisation are negligible with respect to spatial discretisation. The results displayed hereafter correspond to the time level  $T = 2$  seg.

## Results.

The level of accuracy is estimated through the L2 norm of the Entropy error. The Figure 3 displays the results obtained as function of number of degrees of freedom ( $h \sim \sqrt{NDoF}$ , for 2D case). Moreover, the convergence rates for each K value are summarised in the Table 2.

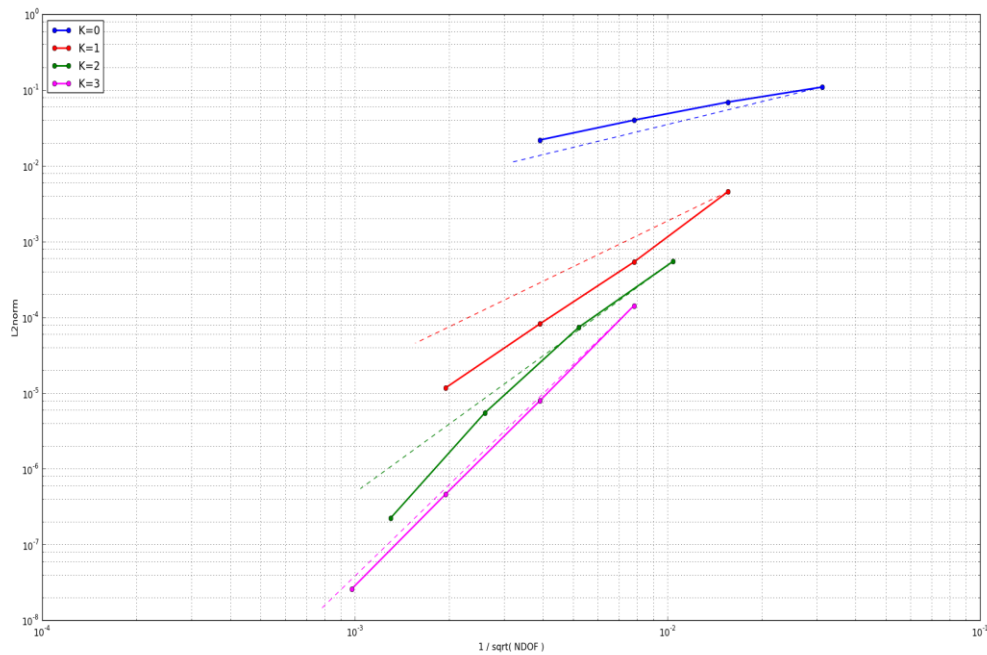


Figure 3: Convergence rates for test case C1.5. obtained with K=0 (blue), K=1 (red), K=2 (green), K=3 (violet). The theoretical slope for each case is sketched as discontinuous line.

<i>Value K</i>	<i>Convergence Rate</i>
0	0.792
1	2.713
2	3.759
3	4.090

Table 2: Convergence rates computed for test case C1.5.